# Effect of PVDF content on the filtration performance and mechanical properties of melt-blown PP fibrous webs

iD Andinet Kumella Eticha[a,b], iD Yasin Akgül[c,d,*], iD Ayben Pakolpakçil[c,e], iD Oğuz Kağan Ünlü[c,f], iD Harun Cüğ[b], and iD Ali Kiliç[c,f]

[a] School of Mechanical and Industrial Engineering, Addis Ababa Institute of Technology, Addis Ababa University, Addis Ababa 385, Ethiopia.

[b] Mechanical Engineering Department, Karabuk University, Karabuk 78050, Türkiye.

[c] Temag Labs, Faculty of Textile Technology and Design, Istanbul Technical University, Istanbul 34437, Türkiye.

[d] Iron and Steel Institute, Karabuk University, Karabuk 78050, Türkiye.

[e] Textile and Fashion Design Department, Faculty of Art and Design, Istanbul Nişantaşı University, Türkiye.

[f] R&D Department, Areka Group LLC, Istanbul, Türkiye.

## ARTICLE INFO

## ABSTRACT

Particulate matter (PM0.3) aerosols are the most penetrating particles, which pose a serious health threat to humans. Therefore, mechanical filtration alone is insufficient to effectively filter 0.3 µm aerosols from a polluted environment. Thus, the need for electrostatic filtration is undeniable. This study aims to investigate the effect of incorporating 10 wt.% and 20 wt.% mass fractions of Polyvinylidene fluoride (PVDF) on the filtration performance and mechanical properties of polypropylene (PP)-based melt-blown (MB) nonwoven filter webs for air filtration applications. Morphological tests, fiber diameter measurements, filtration tests, mechanical tests, contact angle tests, etc., were conducted for each filter web to characterize its properties. The test results revealed that PP/PVDF fibrous webs exhibited thicker micro-fibers in the range of 1.0 to 1.32 µm and rough surface morphologies (beads and droplets) compared to MB PP, which can be attributed to the incorporation of PVDF. Consequently, the introduction of 10 wt.% and 20 wt.% PVDF into PP resulted in the creation of super-hydrophobic MB nonwoven webs, as evidenced by their resistance to water droplets. However, the study also demonstrated that the incorporation of 10 wt.% and 20 wt.% PVDF into PP reduced the tensile strength of PP nonwoven filters by approximately 5.55% and 8.33%, respectively. Furthermore, the addition of 20 wt.% PVDF into PP, along with corona charging, induced a quality factor (QF) of 0.11 mmH2O-1 for the 80PP-20PVDF sample. A similar QF was observed for corona-charged MB PP, which exhibited a filtration efficiency of 99.01% against 0.3 µm aerosol particles, at the expense of a pressure drop of 427 Pa.

## I. INTRODUCTION

Micro/nanofibrous webs emerge as prominent filtering techniques for separating aerosol pollutants of various sizes from polluted environments. These aerosols, in the form of solid and liquid droplets, including toxic PM particles, pose a serious threat to human health [1]. Particles with diameters less than 2.5 µm are particularly hazardous to the respiratory system [2]. Therefore, there is a need for fibrous webs with high filtration performance to improve the quality of inhaled air [3].

Various methods, including electrospinning (ES), solution blow spinning (SBS), centrifugal spinning (CS), and melt-blowing, are used to produce polymeric micro/nanofibrous webs. While ES is low-cost and suitable for lab-scale production [4], it has limitations and is not suitable for industrial-scale manufacturing [3-5]. On the other

side, SBS and CS, driven by air pressure and centrifugal forces respectively, have higher production capacities compared to ES [4, 5]. However, melt-blowing technology surpasses them in terms of production capacity.

Melt-blown nonwovens, known for their high surface area per unit weight, high porosities, and barrier characteristics, are widely used for air filtration. During corona charging, these nonwovens can hold an abundant amount of charges on the fiber periphery, creating a quasi-permanent electric field that attracts negatively charged PM aerosols [6]. Polymers such as polyethylene (PE), polyamide (PA), polyurethane (PUR), poly (ethylene terephthalate) (PET), polystyrene, and poly (butylene terephthalate) (PBT) are suitable polymers types for MB applications [7]. Polypropylene (PP) is commonly used for melt-blown applications due to its versatility, availability, and relatively low cost [8, 9].

Pu et al. [10], studied MB PP using a novel approach of electrostatic-assisted melt-blown technology. In the study, it was found that the average fiber diameter (AFD) obtained from the electrostatic-assisted melt-blown techniques was reduced approximately by 43.19%. Also, the new approach leads to a better filtration efficiency of 50.826% in contrast to the conventional MB method (40.651%) against 0.3 μm aerosol. In another MB PP study, a QF of $1.69 \times 10^{-3}$ Pa$^{-1}$ and a pressure drop of 173 Pa were found by Alberta et al. [11]. Although the filtration efficiency of MB PP filter fabrics increased when thinner fibers were used during the filtration process, there are limitations in the capacity of the device.

Aerosol sizes of 0.3 μm are characterized by the most penetrating particles which cannot be fully filtered by mechanical filtration [12]. To enhance the filtration efficiency of most penetrating small aerosols the need for an electrostatic capturing mechanism along with mechanical filtration is inevitable. Thus, numerous types of research have been done by blending PP with other polymers and electret additives to see their effects on the characteristics of MB nonwoven filter webs. In 2018 Zhang et al. studied MB nonwoven filter webs in detail by preparing PP blended with magnesium stearate (MgSt) as the charge enhancement [6]. The study showed a high filtration efficiency of 99.22% and a low-pressure drop of 92 Pa were achieved with the help of the electret additive. In another research work by Zhang et al. [13], corona-charged MB PP filters exhibit a high filtration efficiency of 99.65% and a pressure drop of 120 Pa. The MB study using Ag@ZIF-8 PP resulted in a filtration efficiency of 88 ± 2.2% and a pressure drop of 51 ± 3.6 Pa against 0.3 μm aerosols [14]. Brochocka et al. [15] studied improving the filtration efficiency of MB PP filters with the effect of electret additives perlite beads (positive charge) and amber (negative charge). An electret perlite-modified PP MB nonwovens exhibit a filtration efficiency of 99.56% and a pressure drop of 290 Pa against sodium chloride aerosols. Previous studies have explored the use of PP and various additives to enhance the filtration efficiency of melt-blown nonwoven filter webs. Some studies have shown promising results by incorporating electret additives or optimizing the fiber web morphology [6, 13, 15]. However, achieving higher filtration efficiency with lower pressure drop remains a challenge.

Piezoelectric polymers such as polyvinylidene fluoride (PVDF) can be used to fabricate melt-blown fibers that exhibit self-polarized electret properties, thus enhancing aerosol filtration [16]. PVDF is known for its low cost, excellent hydrophobicity, and good impact strength [17]. However, there is limited research on melt-blown PP/PVDF filter webs, making it a promising alternative for efficiently filtering 0.3 μm aerosols from polluted environments.

In this study, the effect of different amounts of PVDF on the filtration performance and mechanical behavior of melt-blown PP fibrous webs would be investigated. Additionally, the influence of corona charging on the filtration capacity of PP and PP/PVDF filter webs with the addition of the electret additive zinc stearate (ZnSt) would be examined. Various characterization tests were conducted to gain a better understanding of the behavior of the fabricated filter webs.

## II. EXPERIMENTAL METHOD

### 2.1 Materials

Polypropylene granules with a melt flow index (MFI) of 1800 g/10 min were purchased from TEKNOMELT. Whereas, *Kynar® MG15 resin*-PVDF powder with a density of 1.78 g/cm$^3$ was purchased from ARKEMA. Irgafos-168 powder was purchased from BASF. Maleic anhydride grafted polypropylene (PP-G-mA, MFI = 8 g/10 min) was supplied from DuPont. An electret additive zinc stearate was purchased from BASF.

### 2.2 Methods

#### 2.2.1. Preparation of MB nonwoven filter webs

PVDF fine powders get dried in the vacuum furnace for 2 hrs at 80 °C. Then, as per the DOE presented in Table 1, each composition of MB samples was prepared by blending the dried PVDF powders with other granules. Afterward, sample codes were assigned namely PP, 90PP-10PVDF, and 80PP-20PVDF. The blended compositions for each sample were fed into the extruded compounder (Figure 1) with a twin screw speed of 9 rpm. The compounding process was performed using the process parameter specified in Table 2. For each composition, the extruded compounding process was performed successfully. Subsequently, the MILLER device is used for cutting the compounded PP/PVDF samples into granules. The compounded granules of each sample were again left to dry in a vacuum furnace at 80 °C for another 2 hr to completely remove the presence of any moisture. Later, using the dried compounded granules the MB process for each sample is performed as indicated schematically in Figure 2. Eventually, after the MB process PP, 90PP-10PVDF, and 80PP-20PVDF nonwoven fibrous webs were fabricated. During the fibrous webs production process parameters including screw speed of 12 rpm, die tip-to-collector distance (DCD) of 25 cm, die temperature of 275 °C, hot air pressure of 3 bar, and hot air temperature of 350 °C were used to produce all the nonwoven filter webs.

**Table 1.** Design of experiment (DOE) for MB fiber preparation

| Sample Code | PP (wt.%) | PVDF (wt.%) | Irgafos-168 (wt.%) | ZnSt (wt.%) | PP-G-mA (wt.%) |
|---|---|---|---|---|---|
| PP | 100 | 0 | 1 | 1 | 1.5 |
| 90PP-10PVDF | 90 | 10 | 1 | 1 | 1.5 |
| 80PP-20PVDF | 80 | 20 | 1 | 1 | 1.5 |

**Table 2.** The temperature profile of the twin screw compound extruder

| Heating zone | 1 | 2 | 3 | 4 | 5 | 6 | 7 |
|---|---|---|---|---|---|---|---|
| Temperature *(°C)* | 100 | 150 | 190 | 200 | 210 | 180 | 130 |
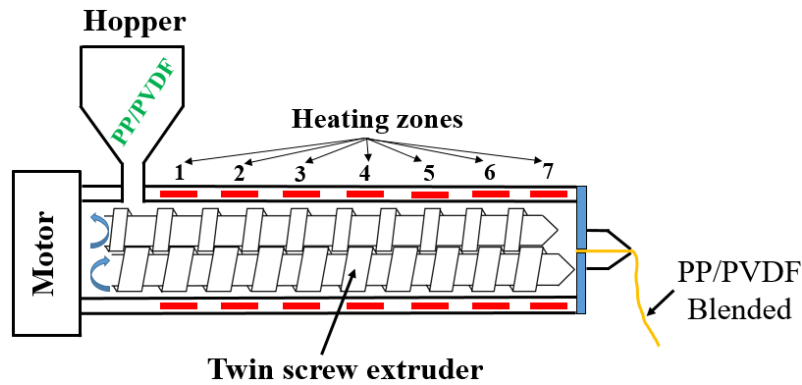
**Figure 1.** Schematic drawing of twin screw compound extruder
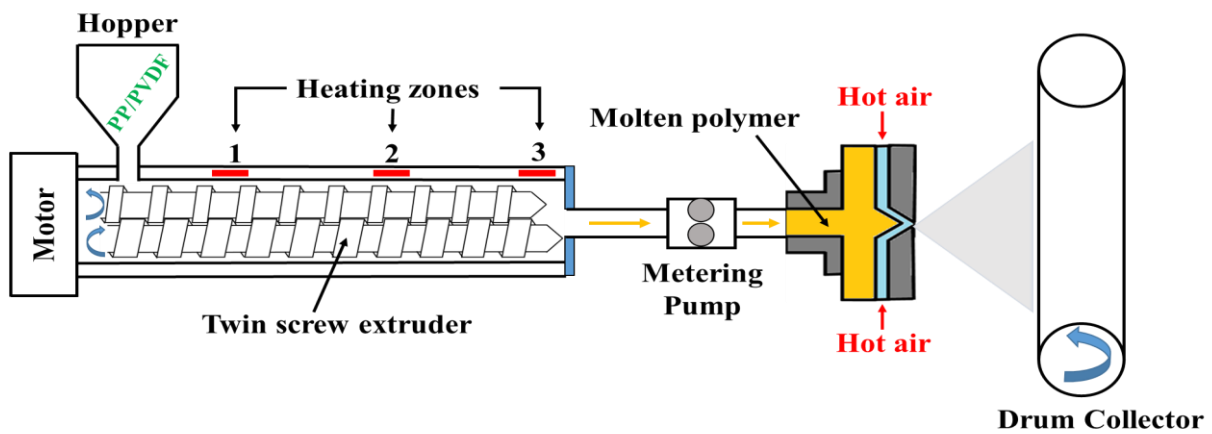


**Figure 2.** Schematic drawing of the MB process

### 2.2.2. Corona charging

The corona charging apparatus schematically represented in Figure 3(a) consists of a high-voltage power supply, two cylindrical rollers separated approximately by 1 mm, a manually rotating handle, and a grounding electrode. Because of the high potential difference between the high-voltage power and the roller-shaped electrode, corona discharge arises, causing the deposition of the positively charged ions on the electret MB fibrous webs. All single-layer samples were charged via a voltage of 2 kV for a charging time of 30 sec. On the contrary, as shown in Figure 3(b) all double-layer nonwoven samples were placed on a plate 5 cm away from the electrode represented by pink color. And for each double-layer MB nonwoven, corona charging is taking place at a higher-voltage power supply of 12.4 kV for 1 min.
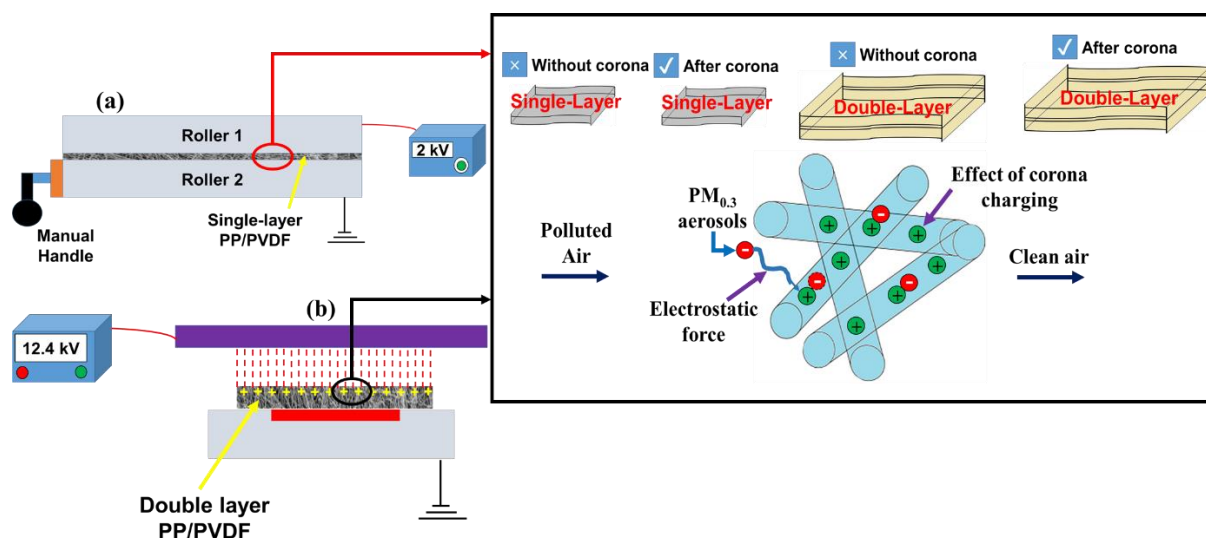
**Figure 3.** Schematic drawing for corona charging of (**a**) single-layer filter webs and (**b**) double-layer filter webs.

## 2.3 Characterization

### 2.3.1. Scanning electron microscope (SEM)

PP and PP/PVDF MB samples were coated with gold via a sputter coater (Quorum, Q150R ES Plus model) and then, fiber morphologies were investigated via Zeiss Ultra Plus scanning electron microscope (SEM). Fiber diameters were determined with the help of ImageJ software. During the fiber diameter determination, a total of 100 random fiber diameter measurements were taken from each sample. Subsequently, for each sample, the measured 100-fiber diameter data would be exported to Origin software for determining the AFD based on the Gaussian approach.

### 2.3.2. Air filtration

The filtration efficiency (η) and pressure drop (ΔP) of MB PP and PP/PVDF filter webs were measured by an automated air filter tester (8130A model, TSI Inc.). Mathematically the filtration efficiency of filter webs was determined by using Eq. 1. On the other side, the filtration performance or QF of each MB filter web is theoretically calculated via Eq. 2. All air filtration tests took place at a 95 l/min flow rate with the help of solid salt (NaCl) particles with a diameter of $0.26 \pm 0.07$ μm at a face velocity of 15.83 cm/s. The tests were conducted three times on each filter sample with an effective area of 100 cm$^2$ to challenge $PM_{0.3}$ NaCl aerosol particles. Each sample's filtration efficiency (η), and pressure drop (ΔP) value is the average of the three individual tests.

$$\eta = 1 - \frac{Cdown}{Cup} \tag{1}$$

where, Cdown and Cup are the captured particles concentration at the downstream and upstream sides, respectively [18].

$$QF = -\frac{\ln(1 - \eta)}{\Delta P} \tag{2}$$

where QF is the representation of the quality factor and $\Delta P$ is the short-hand form of pressure drop [19].

### 2.3.3. Air permeability

PP and PP/PVDF fibrous webs air permeability test was performed according to ISO standards with the help of the Prowhite Airtest II device. The test was performed at room temperature using a fiber filter measuring an area of 38 $cm^2$ and at a constant applied air pressure load of 100 Pa. For each MB filter web air permeability test is conducted five times and the mean of all five tests will be assigned as the air permeability value for each PP and PP/PVDF sample. The air permeability of nonwoven webs is theoretically calculated based on the Darcy equation (Eq. 3).

$$q = \frac{k_p \times \Delta P}{\mu \times L} \tag{3}$$

where q is the representation of air permeability (m/s), $k_p$ is the air permeability coefficient ($m^2$), $\Delta P$ is the short-hand form of pressure drop (Pa), L is samples thickness (m), and $\mu$ is the viscosity of the flow (Pa.s) [20]. Moreover, the air permeability of porous materials can also be computed using Eq. 4.

$$q = \frac{1}{9.4} \times \frac{\Delta P}{\mu \times L} \times \frac{(\rho_f - \rho_n) \times d^2}{\rho_n} \times \frac{2 - lnR_e}{2.4 - lnR_e} \tag{4}$$

where q represents air permeability (m/s), $\Delta P$ is pressure drop (Pa), $\mu$ is flow viscosity (Pa.s), L is the thickness of samples (m), $\rho_f$ and $\rho_n$ are fibers and nonwoven webs densities ($kg/m^3$), d is the diameter of fiber (m), and $R_e$ is the representation of Reynolds number [20].

### 2.3.4. Basis weight measurement

The weight of 10 cm $\times$ 10 cm square-shaped MB fibrous webs was measured by KERN ACJ 220-4M. The basis weight for PP, 90PP-10PVDF, and 80PP-20PVDF samples was determined by dividing the weight of fibrous webs by their effective area as expressed in Eq. 5.

$$BW = \frac{\text{Mass of samples}}{\text{Effective area}} \tag{5}$$

where BW is the designation of samples basis weight.

On the other hand, solidity also known as packing density affects air permeability. Basis weight, the thickness of the filter web, and the density of the fiber material are the major factors that govern solidity. Theoretically, the solidity value of PP, 90PP-10PVDF, and 80PP-20PVDF webs are calculated using the formula given in Eq. 6 [21].

$$Solidity = \frac{BW}{t \times \rho} \tag{6}$$

where t represents the thickness of filter webs and the density of the material, fiber webs are made designated by ρ.

### 2.3.5. Filter web thickness measurement

The thickness of each MB filter web was measured at three different points using LOYKA digital micrometer with a 1 μm measurement resolution. And the mean value was computed and assigned for each sample.

### 2.3.6. Water contact angle (WCA) measurement

To investigate the surface hydrophobicity of filter samples contact angle measurements (Theta Lite) against a drop of nearly 0.0062 ml of pure water at room temperature and pressures were measured by the sessile drop method. For this analysis, samples were prepared with a dimension of 10 mm × 40 mm. Then, three contact angle data at different locations on one surface were averaged to get a reliable value for each sample.

### 2.3.7. Mechanical properties

The mechanical properties of MB fibrous webs with a dimension of 5 cm × 25 cm were investigated according to DIN EN ISO 7198 standard via INSTRON tensile testing device. The test is conducted three times for each MB sample and a mean value was assigned for each PP and PP/PVDF fibrous web. During the test, tensile strength, elongation modulus, and strains were examined under a fiber gauge length of 200 mm and speed of 2 mm/min.

## III. RESULTS AND DISCUSSIONS

### 3.1. SEM morphologies and fiber diameters

In MB technology high-speed hot air stretches the molten polymer to form fine fibers with high porosity. In this study, all nonwoven filter samples were produced under the same MB processing parameters. Figure 4 indicates the MB web morphologies and fiber diameters of PP and PP/PVDF micro/nanofibrous examined under SEM. Although the presence of beads was tremendously high, droplet-free MB filter webs were fabricated for PP (Figure 4(a)). These beads are attributed to the effect of high turbulence of air during MB production [22]. For other nonwoven filters such as 90PP-10PVDF and 80PP-20PVDF randomly distributed fibers with a relatively small

number of droplets were fabricated. But, there were more beaded morphologies were also noticed in 80PP-20PVDF. On the other hand, fibrous webs of AFD 0.62 ± 0.03 μm were examined for melt-spun PP. From the literature survey, it was investigated that by adjusting the MB process parameters such as low screw speed (i.e., low feed rate) and low hot air pressure it can be possible to produce thinner fibers [23]. However, thicker fibers in micro-scale of 1.0 ± 0.03 μm and 1.32 ± 0.07 μm were observed for 90PP-10PVDF and 80PP-20PVDF, respectively. This tells that fiber diameter increases with the increment addition of the content of PVDF into PP. This is attributed to the increment in the viscosity of molten PP/PVDF polymer as compared to PP. Furthermore, fiber diameter distribution for MB samples was considerably influenced by MB process parameters. Also, the amount of blended material PVDF into the host polymer (PP) had a significant effect on fiber diameter distribution. So, PP blended with 10 wt.% PVDF produces narrow fiber distribution with lower fiber diameter as illustrated in Figure 4(b). On the contrary, as indicated in SEM images of Figure 4(c) 20 wt.% PVDF incorporated into PP produces MB webs with higher fiber diameter and wider fiber distribution.
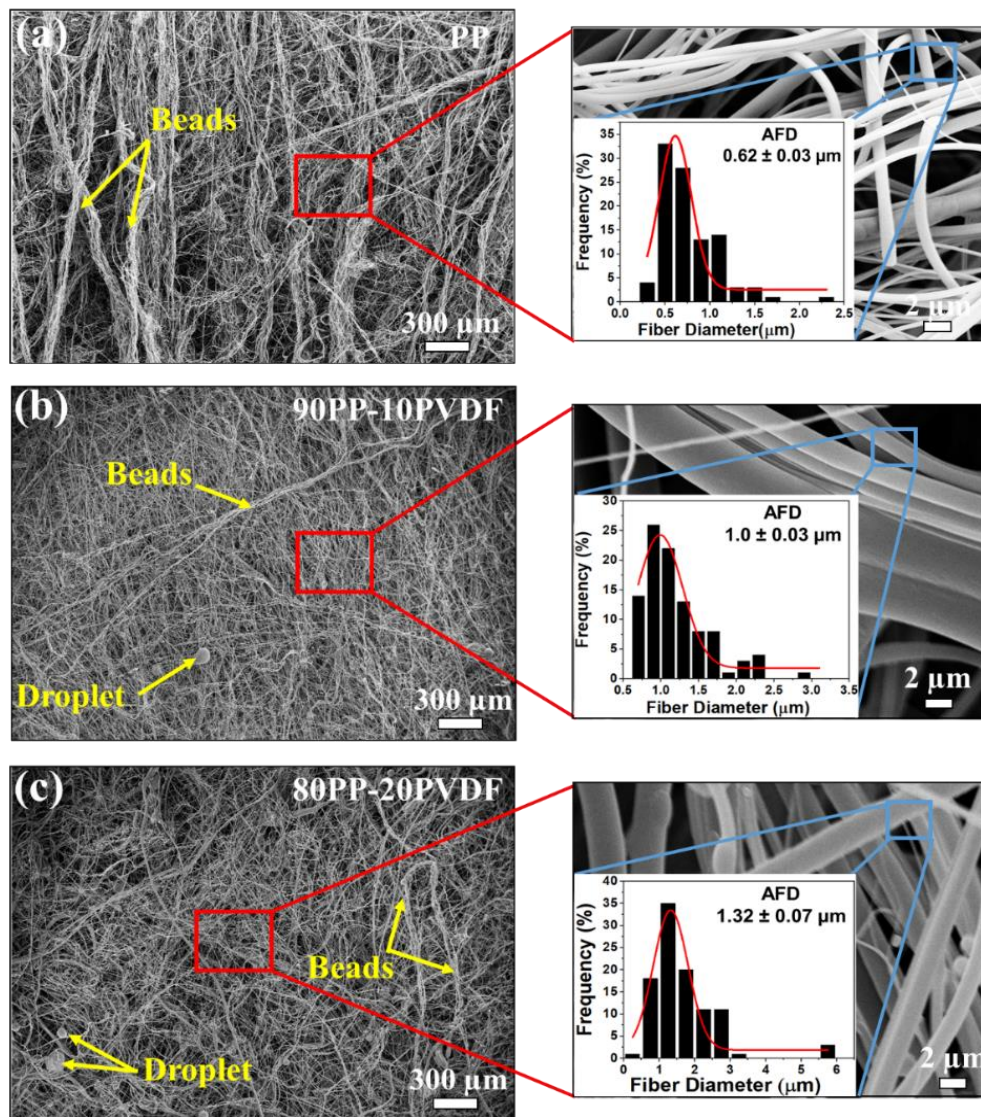


**Figure 4.** Fiber morphologies of MB fibrous webs

### 3.2. Basis weight and air permeability

The basis weight, solidity, and air permeability of single-and-double-layer filter samples were presented in Figures 5(a) and 5(b), respectively. As shown in Figure 5(a) the basis weight for single-layer PP, 90PP-10PVDF, and 80PP-20PVDF was measured as 58.47, 38.96, and 49.62 $g/m^2$, respectively. Similarly, a basis weight value in the range between 77.98 to 116.94 $g/m^2$ was measured for double-layer filter webs as depicted below in Figure 5(b). Compared to MB PP filter webs, PP/PVDF samples blended with 10 and 20 wt.% PVDF showed better air permeability properties. Among single-layer filter webs the highest air permeability of 101.8 mm/s was investigated for the 90PP-10PVDF nonwoven filter, but the lowest is for PP with 81 mm/s. This shows that there exists an indirect relationship between basis weight and air permeability. Looking at Figure 5(a), adding 10 wt.% PVDF into PP results in a 33.37% reduction of basis weight conversely 25.68% improvements were noted in air permeability. Furthermore, the study observed that there were no significant differences were noticed in the air permeability values for filter webs before and after electrification treatment via corona charging. Likewise, a resemble results were noted in the study of Yang et al. [17]. In their study, it was found that filter webs before and after electrification treatment have relatively similar air permeability values. Thickness, density, and fiber diameters are other structural parameters of nonwoven webs which influences filter air permeability. Also, in the literature, it was revealed porosity is another factor that changes the air permeability of MB PP/PVDF nonwoven webs. However, weight is the dominant factor in the determination of air permeability compared to thickness, fiber diameter, and density of fibrous webs [24]. In the study, it was also noted that corona charging had insignificant influence on the air permeability of MB webs.

Similarly, the air permeability test for double-layer filters gives in the range of 16.2 to 39.2 mm/s. The decrement in air permeability values for double-layer MB samples was related to their thickness value in contrast to single-layer filters. Thus, the study showed filter webs thickness had also an influence on their air permeability behavior. The thickness of single-layer nonwoven webs such as PP, 90PP-10PVDF, and 80PP-20PVDF measured as 0.22, 0.72, and 0.74 mm, respectively. On the other hand, thickness values of 0.286, 0.899, and 0.970 mm were reported for double-layer PP, 90PP-10PVDF, and 80PP-20PVDF, respectively. For instance, when filter web thickness was increased from 0.72 to 0.899 mm between single and double layers of 90PP-10PVDF this resulted in an approximately 72.1% reduction in air permeability. Air permeability decrement as a result of increment in filter webs thickness was also noticed in the study of air permeability of Polyester nonwoven fabrics [20]. Generally, due to the less torturous path encountered lower thickness nonwoven webs result in higher air permeability [25]. It was indicated in Figure 5(b) adding 20 wt.% PVDF into PP causes a decrement in basis weight (15.12%) however, the air permeability was enhanced by (142%). The fiber collection time is also another factor that affects fibrous web parameters namely basis weight and thickness but here during fiber production; the collection time for all samples was identical. Basis weight, web thickness, and density of fiber material are the main factors of solidity. An increment in basis weight results in simultaneous enhancement in filter webs solidity but a considerable decrement in air permeability.
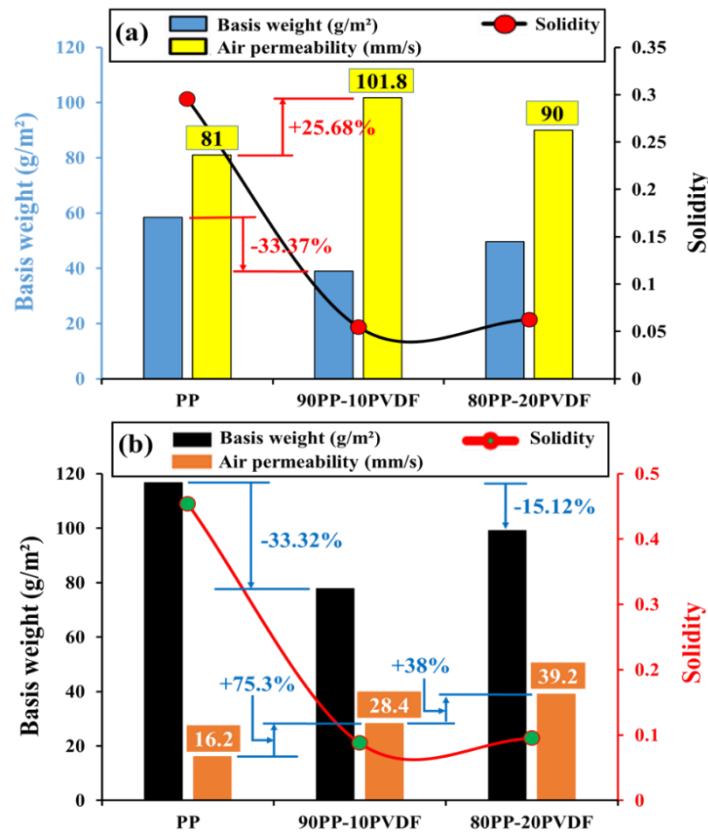
**Figure 5.** Basis weight and air permeability of (**a**) single-layer and (**b**) double-layer MB fibrous webs (where the "+" and "-" signs ahead of the number indicate percentage increment and decrement, respectively)

### 3.3. Filtration Efficiency of MB filter webs

The filtration efficiency test is conducted in single-layer PP, 90PP-10PVDF, and 80PP-20PVDF nonwoven MB filter samples as illustrated in Figure 6(a). Here for each MB sample, the test was performed before and after corona charging. So, from Figure 6(a) it was seen that maximum filtration efficiency of 83.88% and 85.28% were investigated for the PP filter web without corona and after corona charging, respectively. In addition, the maximum pressure drop was also observed for this MB PP sample. This might be due to the effect of beaded morphologies plays a crucial role in enhancing the air resistance properties of the MB PP sample. The highest basis weight for PP samples shows the highest filtration efficiency and pressure drop. The increment in filtration efficiency and pressure drop as a result of enhancement in basis weight was also observed in the study of Liu et al. [26]. On the other side, introducing PVDF into PP-based fibrous webs had considerable effects on reducing the filtration efficiency of PP/PVDF nonwoven filters. Thus, the lowest filtration efficiency of 48.64% was noted for the sample (80PP-20PVDF) produced from the addition of a maximum amount of PVDF (20 wt.%). This might be due to the presence of thicker fiber diameters observed in SEM images and also morphological defects (i.e., droplets and beads) resulting from the addition of PVDF. The reduction in filtration efficiency due to the presence of many thicker fibers was reported in previous research works and hence, this result is supported by past findings. For instance, Eticha et al. showed that the addition of thermoplastic polyurethane (TPU) into electrically assisted solution blow spun PVDF nonwovens results in the reduction of the filtration efficiency of PVDF nanofibrous mats due to the increment in fibers diameter [18].

146

Furthermore, together with mechanical filtration to enhance filtering of the most penetrating particle size of 0.3 μm corona charging technology was adopted on both single-layer (Figure 6(a)) and double-layer (Figure 6(b)) nonwovens. As demonstrated in both Figure 6(a) and 6(b) corona charged samples have shown better filtration efficiency than the uncharged filter webs. This is probably due to charged fibers capturing both charged and neutral aerosol particles with the help of electrostatic force [6]. While considering double-layer fibrous webs before the corona and after corona charging (Figure 6(b)) have exhibited higher filtering efficiency compared to single-layer MB webs (Figure 6(a). This might be due to the increment in the thickness of filter samples. Also, it might be related to because of the higher-voltage power supply and more charging time as compared to single-layer filters. Moreover, in double-layer MB samples, the electret nature of fibers was higher since more charges will be created and stored on the MB webs. Thus, a higher coulomb attraction force is created between charged aerosols and charged fibers, and the electrostatic capturing mechanism will be conducted. On top of that, for neutral aerosols the electric field created by the electret fibers will going to charge the neutral $PM_{0.3}$ aerosols, and filtering action is executed via an electrostatic filtration mechanism. It was also observed that for each corona-charged and uncharged sample, the pressure drop remained relatively the same. This indicates that corona charging does not have remarkable effects on the morphologies of MB nonwoven webs.,
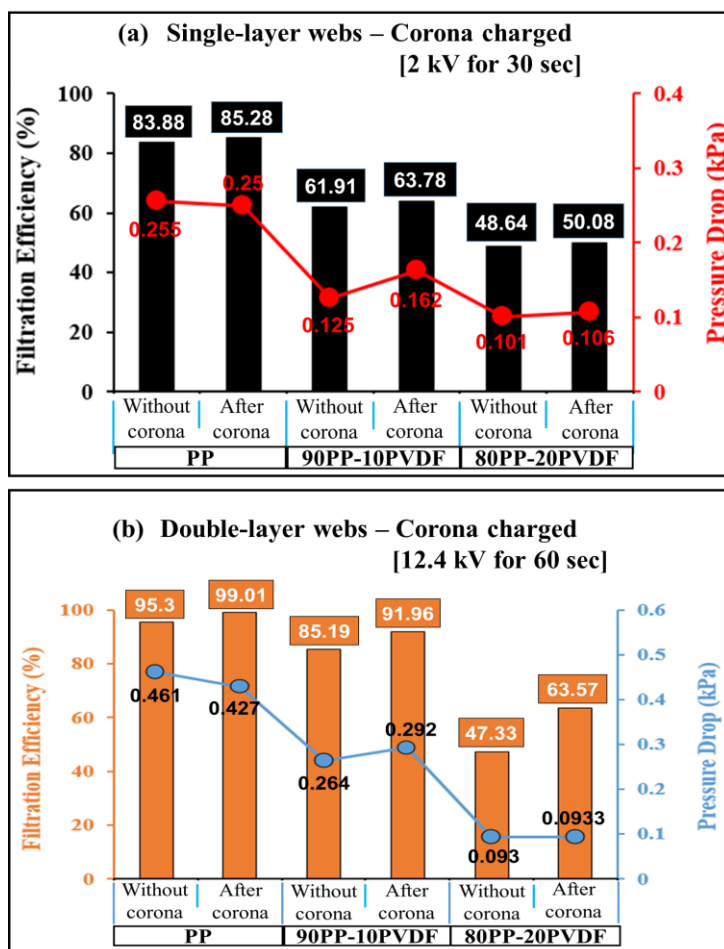


**Figure 6.** Filtration properties of MB filter webs

### 3.4. Filtration performance of MB filter webs

The filtration performance of both single and double-layer MB nonwoven samples PP, 90PP-10PVDF, and 80PP-20PVDF was depicted below in Figure 7. The lowest QF has been noticed for all non-corona-charged MB samples. In addition, as shown in Figure 7(a) blending of PP by a low amount (10 wt.%) of PVDF and without any charging causes a slight improvement in the QF of filter webs than uncharged PP filter samples. But, as the PVDF content increased to 20 wt.% the QF behaves a slight decrement compared to 90PP-10PVDF. This might be related to fiber morphologies (presence of more beads and droplets) responsible for the rising of filters air resistance behavior and an increment in fiber diameter lowers filtration efficiency, the combination of these two scenarios together leads to QF reduction. On the contrary, non-corona charged double-layer MB nonwovens (Figure 7(b)) show the addition of 10 and 20 wt.% PVDF into PP brings about higher QF as compared to PP filters. According to Figure 7(b), corona-charged samples have better QF as compared to uncharged nonwovens. Hence, as indicated in Figure 7(b) the study founds the maximum QF for double-layer corona-charged 80PP-20PVDF samples of 0.11 mmH$_2$O$^{-1}$ at a lower pressure drop of 93.3 Pa. Although corona-charged double-layer PP filter webs have similar QF to double-layer corona-charged 80PP-20PVDF filter sample, it was seen that the measured pressure drop (427 Pa) was remarkably high.

Furthermore, looking at Figures 7(a) and 7(b), generally, the QF value of PP, 90PP-10PVDF, and 80PP-20PVDF is improved by blending PP with 10 and 20 wt.% PVDF contents. Before and after corona charging the QF values for each sample displayed by the bar graph behaves a similar increment trend as represented in Figure 7(b), which shows that the electrostatic force enhances the filtration efficiency without affecting filter webs pressure drop.
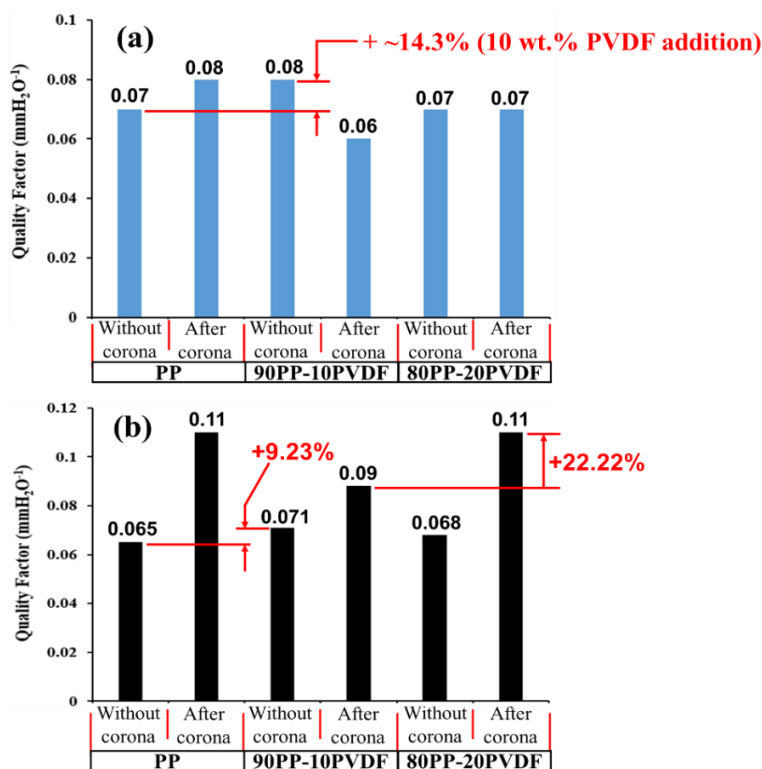


**Figure 7.** Filtration performance of (**a**) single-layer filter webs and (**b**) double-layer filter webs (where the "+" sign ahead of numbers indicates percentage increment)

### 3.5. Contact angle measurements

For each MB filter web sample, the hydrophobicity/hydrophilicity tests were conducted, and their water contact angle values were indicated in Figure 8. Contact angle values of $127.16 \pm 1.52°$, $133.53 \pm 1.52°$, and $134.22 \pm 0.96°$ were measured for PP, 90PP-10PVDF, and 80PP-20PVDF samples, respectively. As per the results, a hydrophobic surface was noticed for all samples. Further, the addition of 10 and 20 wt.% PVDF contents into PP improves the surface hydrophobic character of MB PP nonwoven webs. This is because of the intrinsic hydrophobic characteristics of PVDF [27, 28]. Therefore, the hydrophobic properties of fibrous webs increased with PVDF addition to the PP morphology, and hence, the contact angles increased. In addition to the hydrophobicity of the blended polymer, the surface roughness of filter webs is also another factor that affects the WCA. As shown in SEM images, the introduction of 20 wt.% PVDF results in a large number of beads on the PP/PVDF surface of MB filter webs. So, compared to MB 90PP-10PVDF, SEM images revealed the surface roughness is greater for 80PP-20PVDF, and hence, the surface experience better hydrophobicity properties. This result was in complete agreement with Li et al. [29]. In their study, the addition of PVDF layers into PP shows superior hydrophobicity behavior. A contact angle of 96.96 ° was noted for PP nanofibrous layers, but the WCA value between 100 to 140.5 ° was noted for PVDF-coated PP nanofibrous layers.
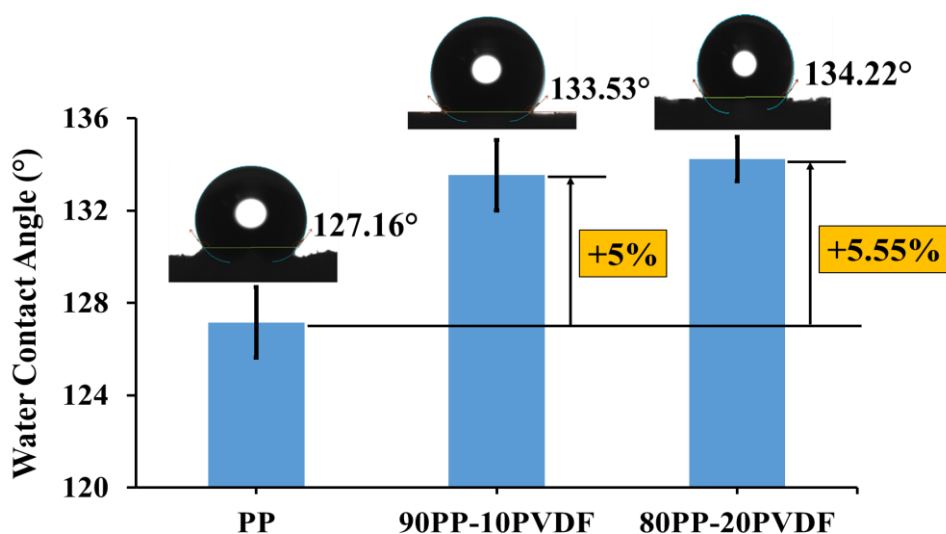


**Figure 8.** MB filter samples with their contact angle values (where the "+" sign ahead of numbers indicates percentage increment)

### 3.6. Mechanical properties

Figure 9 shows the mechanical properties of single-layer MB PP, 90PP-10PVDF, and 80PP-20PVDF fibrous webs. As can be seen in Figure 9(a), the tensile strength slightly decreases with the increment of PVDF content. On the contrary, the addition of 10 wt.% and 20 wt.% PVDF contents into PP notably affect the elastic modulus of the MB PP sample. The maximum tensile strength and elastic modulus were determined for PP with $0.18 \pm 0.05$ MPa and $2.68 \pm 1.08$ MPa, respectively. As the mass fraction of PVDF added to PP is 20 wt.%, the tensile strength and elastic modulus become $0.165 \pm 0.06$ MPa and $1.29 \pm 0.43$ MPa, respectively. The decrement in tensile strength might be attributed to the formation of weak bonds between fibers. Similar mechanical properties were observed

in the studies of PPS/PVDF by Xing et al. [30]. In their study, it was shown that until the content of PVDF reaches 40 wt.% the tensile strength and tensile modulus of PPS/PVDF initially increase for low content of PVDF and then gradually decrease. When the tensile load escalates the nonwoven filter webs begin to fracture gradually as a result of random entanglements of fiber. Strain at break of PP/PVDF MB samples was indicated in Figure 9(b). Incorporation of PVDF (10 and 20 wt.%) into PP reduced the tensile strength and elastic modulus of PP and increased its strain at break. These results were in complete agreement with previous studies by Khakestani et al. [31].
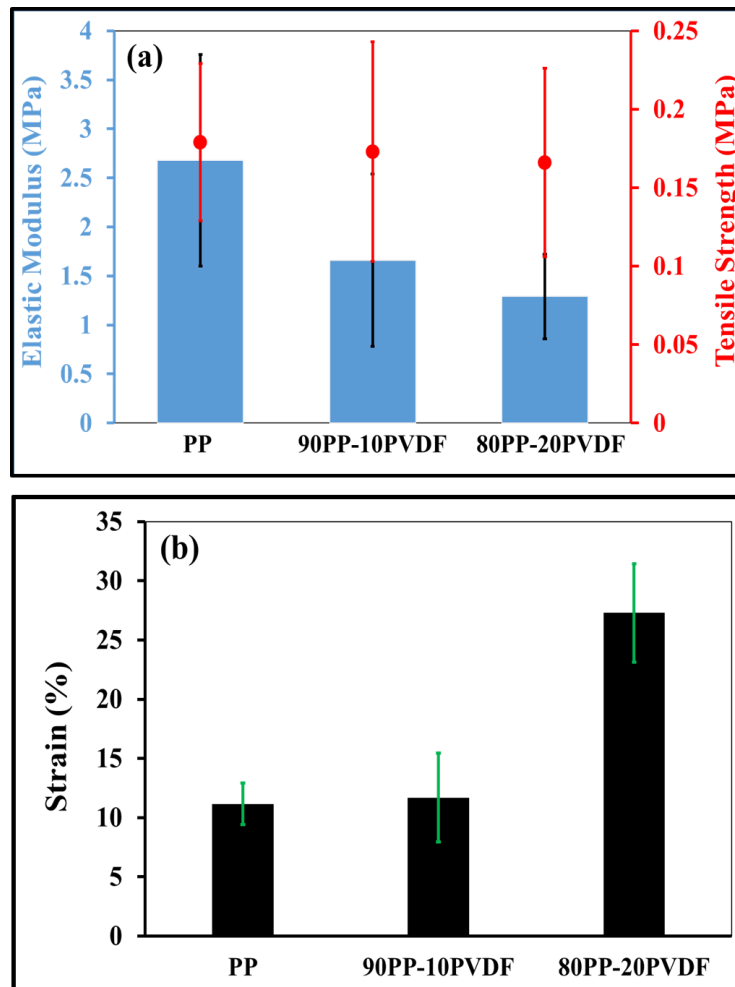


**Figure 9.** Mechanical properties of MB filter webs (**a**) tensile and elastic modulus and (**b**) strain value

## IV. CONCLUSIONS

The fabrication of PP and PP/PVDF nonwoven filter webs using MB technology was successfully achieved. SEM analysis revealed that introducing 20 wt.% PVDF into PP resulted in the production of thicker micro-scale fibers, increased bead formation, and a relatively lower number of droplets compared to the 10 wt.% PVDF composition. The addition of PVDF had a significant advantage in reducing the basis weight of the filter webs, leading to improved air permeability in PP/PVDF samples compared to pure PP filter webs. The piezoelectric properties of

PVDF polymers likely played a crucial role in enhancing the electret characteristics of PP/PVDF filter webs by improving their charge storage capacity after corona charging. Moreover, the incorporation of zinc stearate electret additive in the MB PP and PP/PVDF fibers further enhanced the electrostatic attraction properties of the filter webs. This enhancement was evident in the filtration efficiency results, where the corona-charged PP double-layer filter web exhibited the highest filtration efficiency of 99.01% with a pressure drop of 427 Pa. Corona charging had a remarkable impact on improving PM0.3 aerosol filtration through electrostatic attraction, while not significantly affecting the pressure drops. However, relatively higher pressure drops were observed for the MB samples in this study. On the other hand, the addition of 20 wt.% PVDF significantly improved the hydrophobicity of PP/PVDF nonwovens. Nevertheless, mechanical tests revealed a slight decrease in the tensile and elongation modulus properties of PP-based fibrous webs with the addition of 10 wt.% and 20 wt.% PVDF.

## ACKNOWLEDGMENT

## REFERENCES

[1] Deng Y, Lu T, Cui J, Samal SK, Xiong R, and Huang C (2021) Bio-based electrospun nanofiber as building blocks for a novel eco-friendly air filtration membrane: A review. Separation and Purification Technology 277:119623. https://doi.org/10.1016/j.*seppur*.2021.119623
[2] Mamun A, Blachowicz T, and Sabantina L (2021) Electrospun nanofiber mats for filtering applications—Technology, structure and materials. Polymers 13(9):1368. https://doi.org/10.3390/polym13091368
[3] Zhang X et al. (2021) Multi-layered, corona charged melt blown nonwovens as high performance PM0. 3 air filters. Polymers 13(4):485. https://doi.org/10.3390/polym13040485
[4] Doğan C, Doğan N, Gungor M, Eticha AK, and Akgul Y (2022) Novel active food packaging based on centrifugally spun nanofibers containing lavender essential oil: Rapid fabrication, characterization, and application to preserve of minced lamb meat. Food Packaging and Shelf Life 34:100942. https://doi.org/10.1016/j.fpsl.20222.100942
[5] Doğan N, Doğan C, Eticha AK, Gungor M, and Akgul Y (2022) Centrifugally spun micro-nanofibers based on lemon peel oil/gelatin as novel edible active food packaging: Fabrication, characterization, and application to prevent foodborne pathogens E. coli and S. aureus in cheese. Food Control 139:109081. https://doi.org/10.1016/j.foodcont.2022.109081
[6] Zhang H, Liu J, Zhang X, Huang C, and Jin X (2018) Design of electret polypropylene melt blown air filtration material containing nucleating agent for effective PM2. 5 capture. RSC advances 8(15):7932–7941. https://doi.org/10.1039/c7ra10916d
[7] Bhat G (2015) Meltblown submicron fibers for filter media and other applications. International fiber journal: 20–23.
[8] Duran K, Duran D, OYMAK G, Kilic K, Ezgi Ö, and Mehmet K (2013) Investigation of the physical properties of meltblown nonwovens for air filtration. Textile and Apparel 23(2):136–142.
[9] Han MC et al. (2022) High-performance electret and antibacterial polypropylene meltblown nonwoven materials doped with boehmite and ZnO nanoparticles for air filtration. Fibers and Polymers 23(7):1947–1955. https://doi.org/10.1007/s12221-022-4786-8
[10] Pu Y et al. (2018) Preparation of polypropylene micro and nanofibers by electrostatic-assisted melt blown and their application. Polymers 10(9):959. https://doi.org/10.3390/polym10090959
[11] Podgórski A, Ba\lazy A, and Gradoń L (2006) Application of nanofibers to improve the filtration efficiency of the most penetrating aerosol particles in fibrous filters. Chemical Engineering Science 61(20):6804–6815. https://doi.org/10.1016/j.ces.2006.07.022

[12] Matulevicius J, Kliucininkas L, Martuzevicius D, Krugly E, Tichonovas M, and Baltrusaitis J (2014) Design and characterization of electrospun polyamide nanofiber media for air filtration applications. Journal of nanomaterials. https://doi.org/10.1155/2014/859656

[13] Zhang H et al. (2020) Design of polypropylene electret melt blown nonwovens with superior filtration efficiency stability through thermally stimulated charging. Polymers 12(10):2341. https://doi.org/10.3390/polym12102341

[14] Shiu BC, Zhang Y, Yuan Q, Lin JH, Lou CW, and Li Y (2021) Preparation of Ag@ ZIF-8@ PP melt-blown nonwoven fabrics: air filter efficacy and antibacterial effect. Polymers 13(21):3773. https://doi.org/10.3390/polym13213773

[15] Brochocka A, Majchrzycka K, and Makowski K (2013) Modified melt-blown nonwovens for respiratory protective devices against nanoparticles. Fibres & Textiles in Eastern Europe.

[16] Sanyal A and Sinha-Ray S (2021) Ultrafine PVDF nanofibers for filtration of air-borne particulate matters: A comprehensive review. Polymers 13(11):1864. https://doi.org/10.3390/polym13111864

[17] Yang B, Hao M, Huang Z, Chen Z, and Liu Y (2023) High Filterable Electrospun Nanofibrous Membrane with Charged Electret After Electrification Treatment for Air Filtration. Fibers and Polymers. https://doi.org/10.1007/s12221-023-00110-1

[18] ETICHA AK, TOPTAŞ A, AKGÜL Y, and KILIÇ A (2023) Electrically assisted solution blow spinning of PVDF/TPU nanofibrous mats for air filtration applications. Turkish Journal of Chemistry 47(1):47–53. https://doi.org/10.55730/1300-0527.3515

[19] Gungor M, Toptas A, Calisir MD, and Kilic A (2021) Aerosol filtration performance of nanofibrous mats produced via electrically assisted industrial-scale solution blowing. Polymer Engineering & Science 61(10): 2557–2566. https://doi.org/10.1002/pen.25780

[20] Zhu G, Kremenakova D, Wang Y, and Militky J (2015) Air permeability of polyester nonwoven fabrics. Autex Research Journal 15(1):8–12. https://doi.org/ 10.2478/aut-2014-0019

[21] Leung WWF, Hung CH, and Yuen PT (2010) Effect of face velocity, nanofiber packing density and thickness on filtration performance of filters with nanofibers coated on a substrate. Separation and purification technology 71(1):30–37. https://doi.org/10.1016/j.seppur.2009.10.017

[22] Y. Polat et al. (2019) Solution blown nanofibrous air filters modified with glass microparticles. Journal of Industrial Textiles. https://doi.org/10.1177/1528083719888674

[23] Luiso S, Henry JJ, Pourdeyhimi B, and Fedkiw PS (2020) Fabrication and characterization of meltblown poly (vinylidene difluoride) membranes. ACS Applied Polymer Materials 2(7):2849–2857. https://doi.org/10.1021/acsapm.0c00395

[24] Abuzade RA, Zadhoush A, and Gharehaghaji AA (2012) Air permeability of electrospun polyacrylonitrile nanoweb. Journal of Applied Polymer Science 126(1):232–243. https://doi.org/10.1002/app.36774

[25] Naragund VS and Panda PK (2021) Electrospun polyacrylonitrile nanofiber membranes for air filtration application. International Journal of Environmental Science and Technology. https://doi.org/10.1007/s13762-021-03705-4

[26] Liu B, Zhang S, Wang X, Yu J, and Ding B (2015) Efficient and reusable polyamide-56 nanofiber/nets membrane with bimodal structures for air filtration. Journal of colloid and interface science 457:203–211. http://dx.doi.org/10.1016/j.jcis.2015.07.019

[27] Wu X et al. (2016) Hydrophobic PVDF/graphene hybrid membrane for CO2 absorption in membrane contactor. Journal of Membrane Science 520:120–129. https://doi.org/10.1016/j.memsci.2016.07.025

[28] Francis L, Ghaffour N, Alsaadi AS, Nunes SP, and Amy GL (2014) PVDF hollow fiber and nanofiber membranes for fresh water reclamation using membrane distillation. Journal of Materials Science 49:2045–2053. https://doi.org/10.1007/s10853-013-7894-4

[29] Li H, Shi W, Zeng X, Huang S, Zhang H, and Qin X (2020) Improved desalination properties of hydrophobic GO-incorporated PVDF electrospun nanofibrous composites for vacuum membrane distillation. Separation and Purification Technology 230:115889. https://doi.org/10.1016/j.seppur.2019.115889

[30] Xing J, Ni QQ, Deng B, and Liu Q (2016) Morphology and properties of polyphenylene sulfide (PPS)/polyvinylidene fluoride (PVDF) polymer alloys by melt blending. Composites Science and Technology 134:184–190. https://doi.org/10.1016/j.compscitech.2016.08.020

[31] Khakestani M, Jafari SH, Zahedi P, Bagheri R, and Hajiaghaee R (2017) Physical, morphological, and biological studies on PLA/n HA composite nanofibrous webs containing E quisetum arvense herbal extract for bone tissue engineering. Journal of Applied Polymer Science 134(39):45343. https://doi.org/10.1002/app.45343